Bridging the Gap Between Clinical and Laboratory Label-free Two-photon Excitation Microscopy

Tien Long Dinh[1], Christopher M. Polleys [1], Nilay Vora [1], Hong-Thao Thieu[2], Elizabeth Genega[3] and Irene Georgakoudi [1]
[1] Department of Biomedical Engineering, Tufts University, Medford, MA, USA
[2]Department of Obstetrics and Gynecology, Tufts Medical Center, Boston, MA, USA
[3]Department of Pathology and Laboratory Medicine, Tufts Medical Center, Boston, MA, USA

Acknowledgments:
Professor Eric Miller,
Tufts High-Performance Computing Cluster which was utilized for the research,
Funding:
R01 EB030061, R03 CA235053,
T-Tripod DIAMONDS Program (NSF 1934553),
Tufts University Undergraduate Research Grant

Introduction

- Metabolic perturbation is a prevalent characteristic of many cancers, including cervical cancer[1].
- Mitochondrial organization (MO) correlates with cellular metabolic activity, making it a potential early cancer diagnostic biomarker[2].
- MO is quantitatively characterized using automated analysis of sub-micron resolution reduced nicotinamide adenine dinucleotide (phosphate) (NAD(P)H) two-photon excited fluorescence (TPEF) images[3].
- Clinical label-free TPEF microendoscopes have lower resolution (LR) than lab-bench microscopes and need to be enhanced *in silico* to detect MO-associated precancerous metabolic changes.

Objective:
Developing a to achieve reliable mitochondrial organization assessments in low-resolution NAD(P)H images.

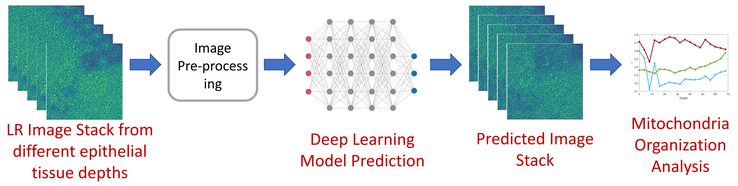

Figure 1: Mitochondrial organization characterization from LR images pathway. The input image stack is pre-processed prior to undergoing transformation by a DL model. The mitochondrial organization is characterized over every 2D image of the predicted image stack.

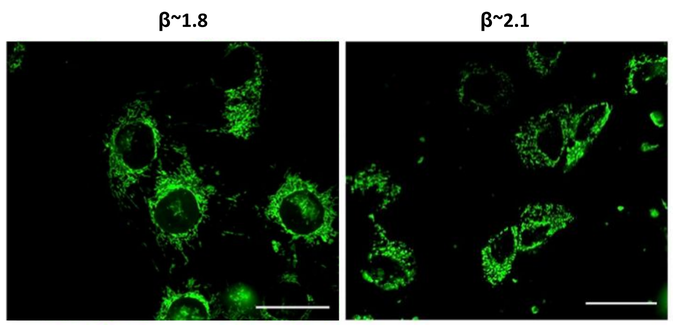

Figure 2: The image with more highly networked mitochondria (left) has a lower β value compared to the image with fragmented mitochondria (right) [4].

Methods

Dataset:

- 15 three-dimensional (3D) stacks of NAD(P)H images (512-by-512-pixels) are acquired from stratified squamous epithelial tissues using a TPEF microscope with 25X (LR) and 40X (HR) objectives and numerical apertures of 0.95 and 1.1, respectively.
- 238 images are preprocessed, registered as pairs of LR and high-resolution (HR) images, and split into training-validation sets with a 4:1 ratio.
- Images are patched into 3808 patches (128-by-128-pixels) for U-Net training.

Methods (continued)

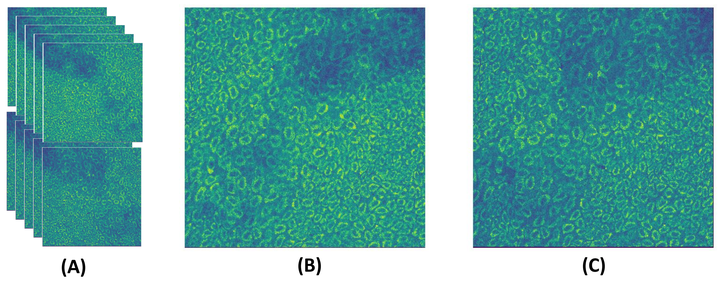

Figure 3: An example of pre-processed image data. [A] The first 5 depths of a pre-processed stack of paired LR and HR NAD(P)H images are shown. Slight variation in brightness is observed in [B] LR and [C] HR pre-processed NAD(P)H images.

Training:

- Standard super-resolution and image restoration metrics are selected for training validation: structural similarity index (SSIM), peak signal-to-noise ratio (PSNR), and their variations.
- Two deep learning models are trained to transform LR images so that MO-associated metrics are similar to those from HR image analysis.
- A supervised deep convolutional neural network (CNN) based on U-net architecture is trained on image pairs[5].
- An unsupervised generative adversary network (GAN) is trained on unpaired training and GT images. The model architecture is based on cycle-consistent adversarial networks (CycleGAN) [6].
- Hyperparameter search and data augmentation is performed to improve training performance.

Analysis:

- Predicted images are visually inspected, and their image similarity to HR is quantitatively assessed.
- MO is characterized using the value of an inverse power law exponent, β, which is fit to the power spectral density of the NAD(P)H images[7].
- β values of LR, predicted, and HR images are evaluated across depths of the tissue stack, and their respective MO trends are compared.

Results

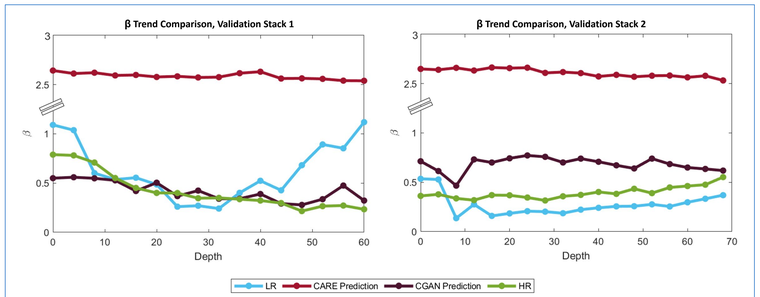

Figure 4: MO characterization of predicted images by U-Net and CycleGAN models compared to the trends of LR and HR images. CycleGAN recovered the HR's β trend in predicted images in stack 1 but mostly preserved LR's trend in stack 2. U-Net significantly altered β intensity and flattened the overall trend in predicted images.

Results (continued)

- Manual inspection of image pairs revealed variability due to changes in the live specimen and non-ideal registration in some image pairs.
- U-Net and CycleGAN models improved the LR images to become more structurally similar to HR images as SSIM increased; however, we observed a decrease in PSNR.
- Visual analysis showed that the U-Net substantially blurred predicted images while CycleGAN reduced the signal contrast in predicted images.
- β trends across all images in image stacks predicted by the U-Net were not recovered. The recovered β trends are nearly flat in all evaluated stacks.
- β trend recovery in predicted image stacks by CycleGAN was inconclusive as MO characterization yielded inconsistent results over evaluated stacks.

Table 1: Quantitative analyses results averaged over the validation dataset

	SSIM	PSNR	β Value
LR	0.261	17.2	0.449
HR	—	—	0.407
U-Net	0.283	16.8	2.60
CycleGAN	0.299	16.2	0.550

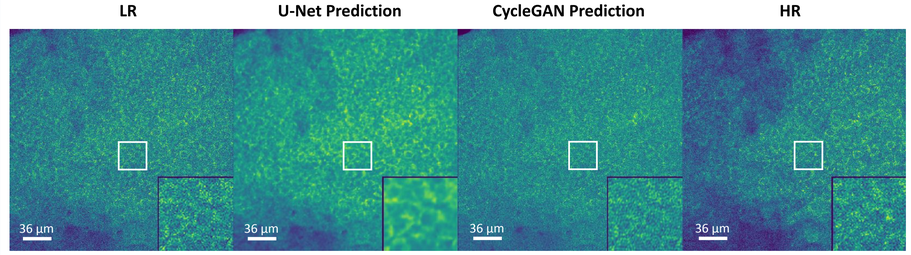

Figure 5 Visual comparison of LR, predictions by U-Net and CycleGAN, and HR of a randomly chosen image from a validation stack. Up-scaled 64-by-64-pixel cropped windows of every image are displayed at bottom right corners.

Discussion

- Changes in SSIM and PSNR metrics do not correlate with improved MO characterization.
- The U-Net model performed poorly on MO analysis over the given dataset. We believe that variations and artifacts in paired images limited the performance of the U-Net.
- CycleGAN improved MO characterization accuracy based on analysis of LR images.
- We hypothesize that CycleGAN's better performance is attributed to the unsupervised training approach, which was not affected by variations in paired images.
- Future studies will focus on collecting new *in vivo* data which will minimize variations in paired images such as tissue shrinkage. Further investigation of unsupervised deep learning methods will be performed on the new datasets.

References:
[1] Vander Heiden MG, Cantley LC, Thompson CB. Understanding the Warburg effect: the metabolic requirements of cell proliferation. *Science*. 2009;324(5930):1029-1033. **[2]** Xylas J, Varone A, Quinn KP, et al. Noninvasive assessment of mitochondrial organization in three-dimensional tissues reveals changes associated with cancer development. *Int J Cancer*. 2015;136(2):322-332. **[3]** Liu Z, Pouli D, Alonzo CA, et al. Mapping metabolic changes by noninvasive, multiparametric, high-resolution imaging using endogenous contrast. *Sci Adv.* 2018;4(3):eaap9302. **[4]** Jheng HF, Tsai PJ, Guo SM, et al. Mitochondrial fission contributes to mitochondrial dysfunction and insulin resistance in skeletal muscle. *Mol Cell Biol*. 2012;32(2):309-319. **[5]** Weigert M, Schmidt U, Boothe T, et al. Content-aware image restoration: pushing the limits of fluorescence microscopy. *Nat Methods*. 2018;15(12):1090-1097. **[6]** Kearney V, Ziemer BP, Perry A, et al. Attention-Aware Discrimination for MR-to-CT Image Translation Using Cycle-Consistent Generative Adversarial Networks. *Radiol Artif Intell.* 2020;2(2):e190027. **[7]** Pouli D, Balu M, Alonzo CA, et al. Imaging mitochondrial dynamics in human skin reveals depth-dependent hypoxia and malignant potential for diagnosis. *Sci Transl Med*. 2016;8(367):367ra169.